

Recent Laboratory Astrophysics Experiments at LULI*

Michel KOENIG¹⁾, Claire MICHAUT³⁾, Bérénice LOUPIAS^{1,2)}, Emeric FALIZE^{2,3)},
Chris GREGORY¹⁾, Yasuhiro KURAMITSU⁸⁾, Seiichi DONO⁸⁾, Tommaso VINCI^{1,2)},
Jonny WAUGH⁴⁾, Nigel WOOLSEY⁴⁾, Norimasa OZAKI⁵⁾, Alessandra BENUZZI-MOUNAIX¹⁾,
Alessandra RAVASIO¹⁾, Serge BOUQUET^{2,3)}, Marc Rabec le GOAHEC¹⁾, Wigen NAZAROV⁶⁾,
Serguey PIKUZ⁷⁾, Youichi SAKAWA⁸⁾, Hideaki TAKABE⁸⁾ and Ryosuke KODAMA⁵⁾

¹⁾LULI, Ecole Polytechnique, CNRS, CEA, UPMC, Route de Saclay, 91128 Palaiseau, France

²⁾CEA-DIF, 91297 Arpajon, France

³⁾LUTH, Observatoire de Paris, CNRS, Université Paris-Diderot, 92190 Meudon, France

⁴⁾Department of Physics, University of York, York, YO10 5DD, U.K.

⁵⁾Graduate School of Engineering, Osaka University, Suita, Osaka 565-0871, Japan

⁶⁾School of Chemistry, University of St Andrews, Purdie Bldg, St Andrews KY16 9ST, United Kingdom

⁷⁾Joint Institute for High Temperatures of RAS, Izhorskaya 13/19, Moscow, 125412, Russia

⁸⁾Institute of Laser Engineering, Osaka University, 2-6 Yamadaoka, Suita, 565-0871, Japan

(Received 16 January 2009 / Accepted 16 March 2009)

At the LULI laboratory we developed since a few years a program on several topics related to laboratory astrophysics: high velocity jets, shock waves in density gradients, collisionless shocks, and radiative shocks (RS). In this paper, the latest experiments related to RS's obtained on the new LULI2000 facility and on GEKKOXII are presented. In particular a strong radiative precursor was observed and its time evolution compared with 2D radiative simulations. The second topic developed at LULI is related to plasma jets which are often observed in Young Stellar Objects (YSO), during their phase of bulk contraction. They interact with the interstellar medium resulting in emission lobes, including the so-called bow shocks. The objective of our experiments was to generate plasma jets propagating through an ambient medium. To this aim, we developed a new target design (a foam filled cone ended with a "nozzle") in order to generate a plasma jet. A jet-like structure was observed and its time evolution studied by varying the foam density. Interaction with ambient medium was recently performed showing growing instabilities for low density gas.

© 2009 The Japan Society of Plasma Science and Nuclear Fusion Research

Keywords: laser-plasma interaction, laboratory astrophysics, radiative hydrodynamics, shock, jet

DOI: 10.1585/pfr.4.044

1. Introduction

Laboratory astrophysics is one of the main applications of high power lasers, especially for the new facilities that are built up such as National Ignition Facility (NIF) or LaserMégajoule (LMJ). Already existing lasers allowed many basic science applications to be performed in particular in the so-called HEDP (High Energy Density Physics) regime in the last decade [1]. Using high power lasers, one can produce matter in an extreme state (high temperature, high density) that can be diagnosed properly and compared to astrophysics situations.

The universe and the wide class of currently well identified astronomical objects (galaxies, stars, interstellar clouds, planets, young star jets, ...) it partly consists in, display a large panel of fascinating phenomena. However up to now, most of them are poorly understood even if recent progresses on astronomical observations brought new

insight in our understanding. Among the major phenomena, radiative shock [2] (RS) and young star jets [3] were recently studied at LULI laboratory with a large worldwide collaboration.

RS plays a special role since it combines both hydrodynamics and radiation physics in a non-trivial way. The major effects occurring during the evolution of various astrophysical objects are driven by these two processes and, although each of them has been widely studied [4], their coupling through the RS is still a source of numerous issues [5]. The radiative properties of astrophysical objects (stellar interiors, accretion shocks, ...) can be very different implying various RS structures.

Jets and collimated outflows are ubiquitous in the Universe associated with the formation of young born stars, planetary nebulae, X-ray binaries or black holes. They consist of elongated plasma structures, including knots, usually bipolar associated with accretion disk around the central source. Through the accretion mechanism from where they originate, jets are the result of a complex

author's e-mail: michel.koenig@polytechnique.edu

*) This article is based on the invited talk at the 14th International Congress on Plasma Physics (ICPP2008).

magneto-hydro-dynamical and radiative process of the collapsing of part of their environment. Jets have long been studied because of their role in removing angular momentum. It involves highly non linear physics coupling magneto-hydrodynamics and radiative transfer.

Experimental RS and jets are of course on much smaller length scales compared to stellar or extragalactic ones as they extend only for a few mm with velocities of order 150 km/s. Nevertheless scaling laws (SL) exist and have been already demonstrated for phenomena which follow a set of equations, like pure hydrodynamic [6], magnetohydrodynamic (MHD) [7] or radiative hydrodynamic systems (optically thin and thick medium) [8, 9]. The scaling law ensures the complete similarity between the astrophysical object and the experiment assuming some conditions. These conditions are the dimensionless numbers which define, by their order of magnitude, the limits of the scaling laws application.

In this paper we first describe how a dynamic astrophysics phenomenon can be linked to a laboratory experiment through appropriate scaling laws. Then two dedicated class of experiments are presented with detailed results and comparison with 2D radiative hydrodynamic simulations.

Relevance to dimensionless numbers is finally discussed.

2. Scaling Laws

Scaling laws validate the laboratory approach that consists in producing phenomena having completely different spatial and temporal scales which are encountered in astrophysical context. This concept is fundamental because it forms the keystone of laboratory astrophysics. This new domain of physics is explicitly based on the concept of universality of the equations and the self-similar character of plasmas. If SL are not explicitly established, one cannot prove similarity between laboratory plasma and its astrophysical counterpart.

In order to establish SL, similarity properties of the phenomena must be examined with a rigorous formalism as already published [6–10]. All this work goes further than dimensional analysis concepts and is performed in astrophysical situations.

First of all, we need to keep hydrodynamic properties between astrophysical and laboratory systems based on three dimensionless parameters which are respectively the Reynolds number Re , the Peclet number Pe , and the Mach number M . The Reynolds number, $Re = vL/\nu$ (where v is the flow velocity, L the characteristic length and ν the kinematic viscosity), gives a measure of the contribution of the inertial forces compared to the viscous forces, and determined if a flow is laminar or turbulent. Since the Peclet number, $Pe = vL/\alpha$ (where $\alpha = \kappa/(\rho c_p)$ is the thermal diffusivity velocity, κ the thermal conductivity, ρ the matter density and c_p the heat capacity), gives the ratio of heat

transported by the flow to heat transported by thermal conduction. The Mach number, $M = v/c_s$ which is the ratio between the flow velocity and the sound speed, indicates if the flow is subsonic ($M < 1$) or supersonic inducing non-linearity in dynamic equations ($M > 1$). For example, young star jets demonstrate high dimensionless hydrodynamic numbers as $Re \gg 1$, $Pe \gg 1$ and $M \approx 10$. For high Mach number ($M \gg 1$) as usually encountered in astrophysics, radiation phenomena occur and have to be taken into account.

Therefore, we also have studied the radiating fluid similarity problem [10] in different radiative hydrodynamic regimes, from optically thin to optically thick, that can be achieved in laboratory with high-power laser facilities. Basing our analysis on Lie group theory, the corresponding SL are derived in each case through a rigorous, exact and quite systematic technique. In optically thick media, we have considered the equilibrium diffusion approximation with the radiative flux F_{rad} and including or not radiative pressure P_{rad} and radiative energy density E_{rad} .

SL are analytical relationships which have been established in all cases, allowing the representation of the considered astrophysical phenomena by rescaled, homothetic, downsized experiments achievable on high-power laser facilities. This rescaling is made possible due to the apparition of free parameters in the transformation that leave invariant the mathematical model under consideration. The number of free parameters depends on the structure of the model and the more we include physical phenomena, the more it is hard to obtain a homothetic system.

Generally, in our experiments of RS and jets performed on LULI2000, the plasma is optically thick, but P_{rad} and E_{rad} are negligible compared to the thermal pressure and matter energy density. However on the Gekko XII case, these quantities, even if too small, can begin to play a role. A classification of radiative regimes applied to RS case has been recently proposed [11]. It is based on 3 dimensionless parameters which are respectively χ the cooling parameter, B_0 the Boltzmann number and R that we decided to call the Mihalas number. These numbers quantify the influence of radiation; in addition of characteristic hydrodynamic quantities v , L , ρ already defined, they depend also on thermal pressure P , adiabatic index γ , internal energy density e and of course radiative quantities. They are related respectively to the ratio between the cooling time and the dynamic one: $\chi = Pv/[(\gamma - 1)F_{\text{rad}}L]$, the flux ratio in material and radiation: $B_0 = (\rho e + P)v/F_{\text{rad}}$, and the energy ratio in material and radiation: $R = \rho e/E_{\text{rad}}$. Let us note that in the case of optically thin media, the χ parameter is written using the cooling function Λ instead of F_{rad} . In our experiments, we find that $\chi \ll 1$ and radiation cooling has to be considered, $B_0 \ll 1$ and the radiative flux has to be taken into account in equation, but $R \gg 1$ so radiative pressure and energy are negligible.

Therefore we will use SL relations for optically thick

plasma in which only the flux F_{rad} for radiation transfer will be considered.

For instance in the case where the radiation flux is given by the heat conduction Spitzer's law, the following relation of F_{rad} is considered:

$$\vec{F}_{\text{rad}} = -K_{\text{rad}} \vec{\nabla} T = K_0 T^{5/2} \vec{\nabla} T$$

where T is the temperature, K_0 is a constant. We have two free parameters a and b given by:

$$a = \rho/\rho' \text{ and } b = P/P',$$

where ρ and P represent the density and the pressure, and where the prime symbol is related to astrophysical system. Therefore, simplified SL relations can be applied for RS:

$$\begin{aligned} x/x' &= a^{-3} b^2, \\ t/t' &= \sqrt{a^{-5} b^3}, \\ v/v' &= \sqrt{b/a}, \\ K_{\text{rad}}/K_{\text{rad}}' &= (b/a)^{2/5}. \end{aligned}$$

3. Radiative Shock

Radiative hydrodynamic processes are very important in several physics areas such as ICF [12] and astrophysics [13–15]. In most astrophysical environments, such as the envelopes of post-AGB stars, a radiative shock is essentially characterized by 1) a hot, ionized, precursor in the upstream material, heated by radiation streaming from high temperature shocked gas, 2) a shock front followed by a short relaxation region between ions, electrons and radiation, and 3) a recombination zone in the downstream flow. In the vicinity of the shock, and for sufficiently high Mach number (M), the precursor is heated to a temperature T equal to that of the shocked material. Shocks with $M > M_{\text{cr}}$ are called supercritical. Since the last decade, several experiments have been performed to simulate radiative hydrodynamic flows of astrophysical interest like jets or blast waves [16] and radiative shocks [2, 17, 18]. However, the lack of various measurements on the same shot could not lead to characterize the radiative shock in a consistent way. The main goal of our recent experiments was therefore to reach RS conditions while performing measurements of fundamental parameters, arising in scaling laws described earlier, with many different initial conditions. In order to obtain the scaling laws, one need to calculate Boltzmann (B_0) and Mihalas (R) numbers defined in Sec. 2. This implies to be able to measure shock velocity and temperature and their respective time evolution in the experiments. To ensure to have radiation effects, it was already shown in a previous paper [19] that RS conditions can be more easily achieved by propagating the shock in a low density medium having a high atomic number. This is the main reason why we did chose xenon as our RS medium for our first set of experiments performed on the LULI2000 laser facility.

The facility consists of two laser beams delivering 450 J at 2ω wavelength in a 1 ns pulse duration. These beams were focused on a 500 μm focal spot providing an intensity on target $I_L \leq 10^{14} \text{ W/cm}^2$. The target was made of an ablator-pusher foil to generate a shock which is then launched into a gas cell containing the xenon. The pusher design was optimized using 1D radiative hydrodynamic simulations (MULTI [20]) according to the laser characteristics. The pusher was made of three layers (20 μm CH-3 μm Ti- 30 μm CH). Following previous work [21], shock velocity up to 60-70 km/s can be obtained giving on upper limit on the xenon gas initial pressure $P_{\text{xe}} < 1 \text{ bar}$ ($5 \cdot 10^{-3} \text{ g/cm}^3$). We decided, therefore, to use different initial pressure values ($P_{\text{xe}} = 0.1\text{-}0.3 \text{ bar}$) and different initial laser intensities to cover various radiative regimes.

Two main sets of diagnostics were implemented: on the rear side of the target, a streak camera (“Self Emission”) collected photons emitted by the target giving the shock temperature. We had also two rear side VISAR [22] to infer shock velocity in the CH pusher (LULI2000 case). On the transverse axis, the cell is probed by a low power laser pulse ($\lambda = 532 \text{ nm}$, $\Delta t = 8 \text{ ns}$) injected into a VISAR system [23]. These interferometers, based on change in index of refraction, led to the measurement not only of the electronic density but also both shock and precursor velocities. In the most recent experiments, two Gated Optical Imager (GOI) imaged, by visible shadowgraphy, the 2D shape of the shock at different times (120 ps time resolution).

The various diagnostics we implemented in these experiments, allowed us to measure several relevant and consistent parameters for the description of the radiative shock such as the shock and precursor velocities, their respective temperatures and the electron density in the precursor. Moreover we also determine the radial evolution of the shocked material which is a good indication of the radiative losses.

Regarding the shock velocities, the measured values depend on the initial conditions, i.e., laser intensity on target and initial pressure of the gas: they range from 50 to 80 km/s increasing with laser energy. The same trend occurs for the temperature ranging from 10 to 20 eV. However for this parameter, the initial density plays an crucial role as half of energy coming from the shock is converted to internal energy, which means higher temperature for lower density. In those experiments, we almost achieved the condition $B_0 \leq 1$ ($0.4 < B_0 < 4$) which is necessary to obtain a radiative precursor. But the laser energy was not high enough to enter the full radiative regime where $R < 1$ (here $200 < R < 3000$). In order to detect the radiative precursor and its time evolution, a visible shadowgraphy diagnostic coupled to GOI's was used. An example is shown in Fig. 1, where we do observe the shock front (opaque behind) and the precursor (a 200-300 μm layer between 0.4-0.7 mm of absorbed light in front of it).

This absorption, typically 20-30%, is due to the ioni-

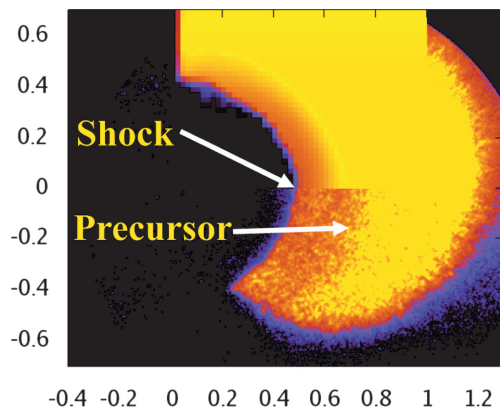


Fig. 1 GOI image at $t = 11$ ns. On the upper part, the 3D reconstructed image is shown. The color level stands for probe laser absorption in the gas.

sation of xenon in front of the shock (i.e. in the precursor) due to the shock front radiation. Therefore we could determine the precursor temperature as long as a set of opacities (at the probe beam wavelength = $0.53 \mu\text{m}$) for different temperatures is known (the density in precursor being the initial density). One possibility is to use a free-free model for the opacity as done for shock temperature checked previously in comparison with detailed configuration calculation [24]. Here the absorption parameter κ (cm^{-1}) is directly linked to the ionisation degree Z^* and the temperature. Following a recent paper [25], $Z^* \approx 20 T^{0.5}$ so κ depends now only on the temperature and a direct determination of the precursor temperature can be made. Values ranging from 13 to 20 eV are deduced for absorption between 20% and 30% respectively.

On the upper part of the figure, a 3D reconstructed image is presented which comes from a 2D radiative hydrodynamic simulation coupled to a postprocessed ray-tracing code. Even if very useful and important data were obtained from these experiments using gas, a more radiative regime must be achieved. To overcome the lack of laser energy, we performed new experiments on the GEKKO XII laser facility. Here a new target scheme, already proposed by Bozier *et al.* [17], was implemented which consists of a tube filled of low density (50 mg/cc) foam directly irradiated by the laser. In this case, the pressure generated in the foam is the so-called ablation pressure which could reach, for intensities on target achievable on GEKKOXII ($I_L \leq 510^{14} \text{ W/cm}^2$), 50 Mbar. For such a high value of pressure, shock velocity and temperature are expected to be around 300 km/s and 350 eV respectively giving $B_0 = 0.2$ et $R = 30$. In our experiment, two main diagnostics were implemented both working in the X-ray domain. First a self-emission (above 1 keV) imaging of the heated foam, second a radiograph of the shock propagating in the tube using vanadium He α backlighter (5.1 keV). Both of these diagnostics were coupled to a streak camera to follow the time evolution of the shock front.

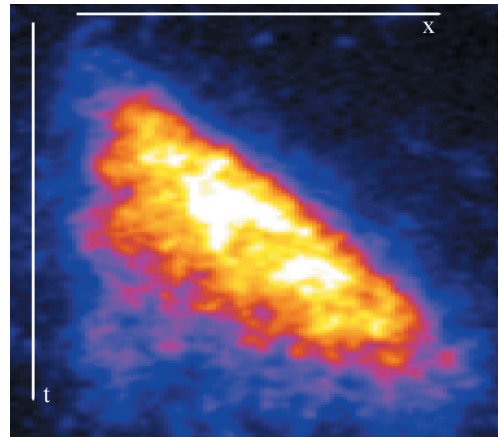


Fig. 2 Streaked X-ray self-emission of the heated foam. The velocity (170 km/s) corresponds to the ablation front.

In the experiment, only one diagnostic was working properly so we could observe x-ray self-emission (Fig. 2) arising from the ablation front which is heated by the laser beam up to 1 keV or more. The velocity of this high temperature front is 170 km/s whereas the shock velocity is expected to be higher (> 250 km/s). Comparison with radiative hydrodynamic simulations shows good agreement and indicates important effects due to radiation losses such as shock deceleration.

4. Astrophysical Jets Experiment

Astrophysical jets take place in astronomical systems exhibiting accretion disk such as young stellar objects (YSOs), supernovae, pulsars, active galactic nuclei and so forth. Whereas from these systems the launching could be different, the jets share some common characteristics (morphology) [26]. Experiments such as those discussed below are aimed to produce laboratory plasma jets using intense laser to approach YSOs jets problematic. We pay a particular attention to measure the jet parameters (density, temperature and velocity) in order to gain useful information and to determine the dimensionless parameters to validate the similarity criteria. The YSOs during their formation need to release energy to pursue their contraction to initiate the thermonuclear fusion. This is achieved thanks to the high amount of matter ejection in bipolar outflows. During the generation of the plasma jet, MHD processes seem to be the most promising candidate to recreate the observational characteristics of YSO. It also remains questions concerning the jet propagation and its interaction with the interstellar medium (ISM) where magnetic field seems to be negligible [27]. In the presented experiments we study the plasma jet propagation in these conditions and it concerns the regions having little or no magnetic effects, ie from 300 AU from the source. Our ability to provide useful information for astrophysical problems is possible if similarity criteria can be experimentally checked. It is

achieved using a large panel of diagnostics allowing a full characterization of the plasma jet evolution. We first sum up the main results concerning our plasma jet propagation in vacuum and secondly we present its interaction with an ambient medium which simulates the ISM.

4.1 Jet propagation in vacuum

In this section we sum up the major results we have obtained for plasma jet propagation in vacuum [3]. All these measurements allow to accurately describe the jet and to calculate its dimensionless parameters.

The two LULI2000 kJ nanosecond beams were converted at 2ω to drive a strong shock through the target and were focused with a $500\ \mu\text{m}$ focal spot diameter giving a laser intensity $I_L \sim 10^{14}\ \text{W}/\text{cm}^2$ (pulse duration 1.5 ns). The target was made of a solid pusher glued on the entrance hole of a cone filled of foam. The shock was guided by the cone walls and formed the plasma jet along the cone axis. A washer ($100\ \mu\text{m}$ length and $100\ \mu\text{m}$ diameter hole) was attached to the rear side of the target to increase the plasma collimation for the initial stage of the expansion. The plastic foam density ranged from $20\ \text{mg}\cdot\text{cm}^{-3}$ to $200\ \text{mg}\cdot\text{cm}^{-3}$ was brominated in mass up to 30% for x-ray diagnostics purpose.

Jet velocity was measured using transverse visible shadowgraph ($\lambda = 532\ \text{nm}$) or transverse self optical pyrometer ($\lambda = 450\ \text{nm}$). The velocity time evolution of the plasma jet in vacuum, for a given initial foam density, is linked to the shock conditions in the foam, and a proper adjustment of the laser focal spot at the cone entrance. The shock acceleration in low density foam target is produced by impedance matching for different densities of foam (identical laser intensity and pusher). The jet velocity ranged from $90\ \text{km}/\text{s}$ for $200\ \text{mg}\cdot\text{cm}^{-3}$ foam density to $178\ \text{km}/\text{s}$ for $20\ \text{mg}\cdot\text{cm}^{-3}$. We also measured an acceleration of the jet with the addition of the washer, while the addition of bromine has no effect on the velocity.

The radial evolution of the jet was also measured either by using transverse visible shadowgraph with GOI or by rear side self optical pyrometer. This last diagnostic allowed inferring jet temperature using an absolute photon counting technique to get the equivalent blackbody temperature. We observed a radial expansion of the plasma and measured its velocity which ranged from $22\ \text{km}/\text{s}$ to $52\ \text{km}/\text{s}$. This radial evolution is determined by the plasma jet temperature [28] and is also linked to the shock conditions in the cone. Finally using both X-ray radiography and visible interferometer we could determine the plasma jet density. At the beginning of the plasma jet propagation in vacuum, X ray absorption provides the denser part of the jet and we estimate an average density $\sim 0.2\ \text{g}/\text{cc}$. This measurement demonstrates an important collimation of the foam by the cone. For longer delay, the plasma expansion in vacuum allows to measure the electron density (n_e) using a Mach-Zehnder interferometer [29] (Fig. 3).

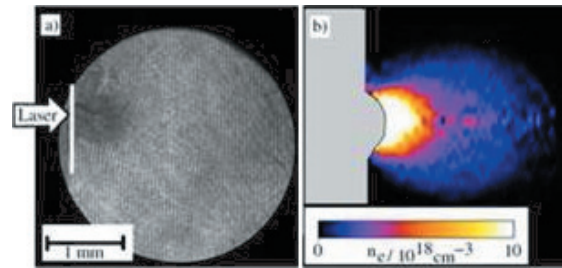


Fig. 3 (a) Interferogram of the plasma jet for 30 ns delay. (b) Electron density map of the plasma using Abel inversion.

Using this panel of measurements and for this particular shock condition in the foam target we determined the jet dimensionless parameters: $M \sim 10$, $Pe \gg 1$, $Re \gg 1$, and $\chi \gg 10$ (cooling factor using blackbody law as lower limit for radiative time). Typical astrophysical jet parameters are $M \sim 10$, $Pe \gg 1$, $Re \gg 1$, and $\chi \sim 0.1-10$. Therefore, we were able to generate high Mach number low temperature jets having good similarities with astrophysical jets. However, as it evolves into vacuum and is optically thick, χ is larger than the scaling parameter for YSO jets. Finally, as this first experiment was focused on plasma jet formation, a last dimensionless number was not accessible: the density ratio between the plasma jet density and the ISM density η .

4.2 Jet propagation in an ambient medium

In this section, we present recent results of the jet propagation in an ambient medium. Here the goal was to reach astrophysical conditions by simulating the ISM effects in the plasma jet propagation and to observe the formation of the so-called bow shock structure. This shock appears at the head of the jet when it propagates through the ISM with a very perturbed and fragmented shape [30]. The evolution of the bow shock is not clearly understood for the moment.

As for previous experiment, we used a long pulse beam to generate the plasma jet but also a short pulse beam ($100\ \text{J}$ in $1\ \text{ps}$) to produce high energy protons for a dedicated radiography. The target was the same as the one used to study jet propagation in vacuum. All previous visible diagnostics as described above were also available. In order to simulate the ISM, a gas jet nozzle at the rear side of the target was used. The gas nozzle pressure was varied from 5 bar to 80 bar, resulting in an argon (Ar) number density ranging from $6 \times 10^{17}\ \text{cm}^{-3}$ to $1 \times 10^{19}\ \text{cm}^{-3}$.

Unlike in the case of the jet evolution in vacuum, there are two main modifications for the visible transverse emission: the plasma velocity decreases and the intensity is modulated (Fig. 4).

We clearly observe a deceleration of the velocity from $115\ \text{km}/\text{s}$ to $80\ \text{km}/\text{s}$. We also notice particular emission

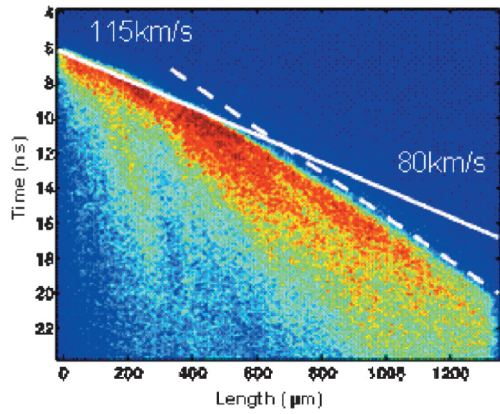


Fig. 4 Velocity measurements from transverse SOP.

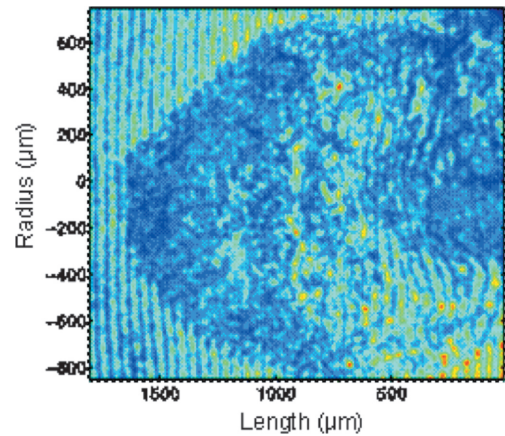


Fig. 6 Visible interferogram of the plasma jet interaction with an ambient medium (delay 30 ns, $\eta = 2.5$).

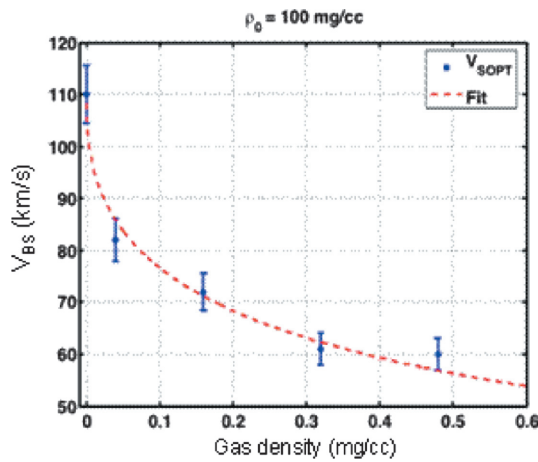


Fig. 5 Velocity measurements using transverse SOP at different ambient gas density are presented in blue. The red curve corresponds to the best fit using Eq. (1).

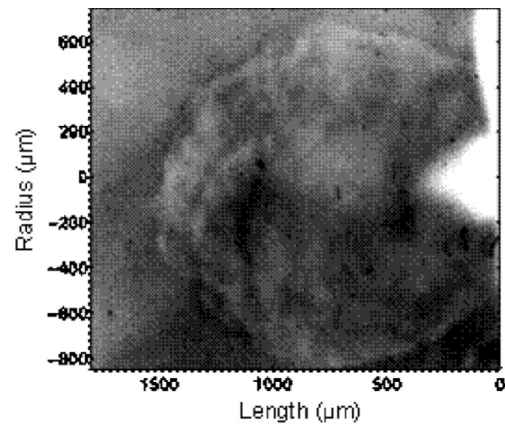


Fig. 7 Proton radiography of the plasma jet interaction with an ambient medium (delay 30 ns, $\eta = 2.5$).

profiles (at fixed time) which show an intensity increasing along the jet. In comparison, for a shot without gas, a roughly constant emission level all along the jet is observed.

These two features allow us to conclude that the velocity measured in the presence of an ambient medium comes from the shock front generated by the interaction of the plasma jet with the gas: the bow shock. Its velocity (V_{BS}) varies according to the jet density (n_j), the ambient medium (n_a) and the jet velocity (V_j) [30]:

$$\beta n_j (V_j - V_{BS})^2 = n_a V_{BS}^2, \tag{1}$$

where β corresponds to the momentum transfer efficiency and ranges from 0.4 to 0.8.

By measuring the bow shock velocity for different ambient medium density (blue points in Fig. 5) and using the best fit following Eq. (1) (red curve in Fig. 5) we could deduce the jet density: n_j . The last dimensionless parameters: $\eta = n_j/n_a$ can then be inferred. Hence in our experiment, by investigating different ambient density n_a , we were able

to deduce the density ratio range: $2.5 < \eta < 22$. Which is close to the astrophysical case ($\eta = 1-10$).

Thanks to the transverse visible interferometer and the proton radiography we observed very interesting structure regarding the jet frontiers interacting with the gas. The visible interferogram (Fig. 6) shows an opaque part at the limit between the jet and the ambient medium. But we can observe, close to the target (position $x = 0 \mu m$), fringes pattern indicating a lower electron density that allow the probe beam to be transmitted. This is due to the plasma jet expansion occurring at long delay (30 ns) which corresponds to the snapshot presented here (Fig. 6). The opaque region all around the jet corresponds probably to the bow shock and appears perturbed but without any details on these structures.

In addition to visible interferometry, the proton radiography allowed to point out accurately these structures (Fig. 7). After propagation through the jet, the proton beam was detected by a Radiocromic Film (RCF) multi-layer stack. Each film selects a narrow band of proton en-

ergies, leading to a spectral capability of the multilayer detector. In Fig. 7, the radiograph (corresponding to 5 MeV protons) shows the same perturbations with same dimensions as in the visible interferogram (Fig. 6). The shape of the perturbed envelope of the interaction zone between the jet and the gas is delimited by a deflection and absorption of protons. The high spatial resolution ($\sim 20 \mu\text{m}$) and time resolution ($5 \pm 2 \text{ MeV}$) allowed to observe clearly the structures generated by the interaction between the jet and the ambient gas. These results are still under analysis.

5. Conclusions

Laboratory is a new fast growing activity with respect to the development of large scale laser facilities. The correspondence between astrophysical objects or situations and experiment can be ensured when scaling laws apply. In that case, dimensionless numbers such as Mach number (M), cooling parameter (χ), Boltzmann (B_0) or Mihalas (R) numbers have to match between the two systems. Regarding RS, we have observed, at the LULI2000 facility, the development of a radiative precursor ahead a strong supercritical shock wave, in a xenon gas cell at low pressure. We have been able to measure simultaneously fundamental parameters such as radial expansion, electron density, shock and precursor velocities and temperatures. Measurements have been performed with different initial conditions (by varying the laser energy and the xenon initial pressure). Comparison with simulations shows good agreement in all the detailed behaviour of the radiative shock especially in the influence of radial expansion due to radiation.

Acknowledgment

The authors would like to acknowledge the support from the CNRS-JSPS joint project N° 195, the JSPS core-to-core program and the joint CNRS-RAS project N° 165.

CDG acknowledges financial support from Région Ile-de-France.

- [1] B.A. Remington *et al.*, *Rev. Mod. Phys.* **78**, 755 (2006).
- [2] S. Bouquet *et al.*, *Phys. Rev. Lett.* **92**, 225001 (2004).
- [3] B. Loupias *et al.*, *Phys. Rev. Lett.* **99**, 265001 (2007).
- [4] H. Lamb, *Hydrodynamics* (Cambridge University Press, 1994).
- [5] D. Mihalas and B.W. Mihalas, *Foundations of radiation hydrodynamics* (Dover Publications. N.Y., 2000).
- [6] D.D. Ryutov *et al.*, *Astrophys. J.* **518**, 821 (1999).
- [7] D. Ryutov *et al.*, *ApJS supplement series* **127**, 465 (2000).
- [8] D.D. Ryutov *et al.*, *Phys. Plasmas* **8**, 1804 (2001).
- [9] E. Falize *et al.*, *J. Phys. Conf. Ser.* **112**, 042016 (2008).
- [10] E. Falize *et al.*, *Astrophys. Space Sci.* **322**, 107 (2009).
- [11] C. Michaut *et al.*, *Astrophys. Space Sci.* **322**, 77 (2009).
- [12] J.D. Lindl *et al.*, *Phys. Plasmas* **11**, 339 (2004).
- [13] S.K. Chakrabarti and L.G. Titarchuk, *Astrophys. J.* **455**, 623 (1995).
- [14] A.V. Farnsworth and J.H. Clarke, *Phys. Fluids* **14**, 1352 (1971).
- [15] R. Sivron *et al.*, *Astrophys. J.* **469**, 542 (1996).
- [16] M.J. Edwards *et al.*, *Phys. Rev. Lett.* **87**, 085004 (2001).
- [17] J.C. Bozier *et al.*, *Astrophys. J. Supp.* **127**, 253 (2000).
- [18] A.B. Reighard *et al.*, *Phys. Plasmas* **13**, 082901 (2006).
- [19] S. Bouquet *et al.*, *Astrophys. J. Supp.* **127**, 245 (2000).
- [20] R. Ramis *et al.*, *Comp. Phys. Comm.* **49**, 475 (1988).
- [21] M. Koenig *et al.*, *Appl. Phys. Lett.* **75**, 3026 (1999).
- [22] P.M. Celliers *et al.*, *Applied Phys. Lett.* **73**, 1320 (1998).
- [23] M. Koenig *et al.*, *Phys. Plasmas* **13**, 056504 (2006).
- [24] O. Peyrusse, *J. Physics B* **33**, 4303 (2000).
- [25] R.P. Drake, *Astrophys. Space Sci.* **298**, 49 (2005).
- [26] E.M. de-Gouveia-dal-Pino, *Adv. Space Res.* **35**, 908 (2005).
- [27] P. Hartigan *et al.*, *Astrophys. J.* **661**, 910 (2007).
- [28] E. Falize *et al.*, *J. Phys. Conf. Ser.* **112**, 042015 (2008).
- [29] C.D. Gregory *et al.*, *Plasma Phys. Contr. Fusion* **50**, 124039 (2008).
- [30] P. Hartigan, *Astrophys. J.* **339**, 987 (1989).